



# Energy-Based Brittleness Index and Acoustic Emission Characteristics of Anisotropic Coal Under Triaxial Stress Condition

Jun Zhang<sup>1</sup> · Chi Ai<sup>1</sup> · Yu-wei Li<sup>1</sup> · Ming-guang Che<sup>2</sup> · Rui Gao<sup>2</sup> · Jia Zeng<sup>3</sup>

Received: 17 July 2017 / Accepted: 16 June 2018 / Published online: 3 July 2018  
 © Springer-Verlag GmbH Austria, part of Springer Nature 2018

## Abstract

Evaluating the ability of coal seams to form fracture networks by hydraulic fracturing is important for the development of coalbed methane (CBM) reservoirs. In this paper, a new index for evaluating coal brittleness was established from the perspective of energy evolution during coal failure. Uniaxial and triaxial compression tests of coal monitored by an acoustic emission (AE) system were carried out and the applicability of the new index and the influence of the confining pressure and cleat orientation on the coal brittleness were analyzed. The pre-peak and post-peak dissipated energies were the essential factors in determining the coal brittleness. The new index can characterize the influence of the external stress and cleat orientation on coal brittleness, and can also comprehensively reflect the mechanical properties of the coal during the pre-peak and post-peak stages. The corresponding AE energy curves can be divided into *Rapid Fracture Type*, *Stable Fracture Type* and *Plastic Fracture Type*. For the *Rapid Fracture Type*, the accumulation rate of AE energy showed sudden changes when reaching the yield stress and peak strength, which represented high brittleness. The *Plastic Fracture Type* represented low brittleness, and the accumulated AE energy curves were smooth—first concave and then convex. The brittleness index of coal studied in this paper can provide a new method for selecting the optimal CBM reservoir and optimizing the fracturing scheme.

**Keywords** Brittleness · Hydraulic fracturing · Coalbed methane reservoir · Strain energy · Acoustic emission energy

## List of symbols

YM_BRIT = ( $E - E_{\min}$ )/( $E_{\max} - E_{\min}$ )	$E_{\max}$ and $E_{\min}$ are the maximum and minimum values of elastic modulus ( $b_1$ )	$\sigma_c, \sigma_t$	The uniaxial compressive strength and the tensile strength ( $b_3$ )
PR_BRIT = ( $v - v_{\max}$ )/( $v_{\min} - v_{\max}$ )	$v_{\max}$ and $v_{\min}$ are the maximum and minimum values of Poisson's ratio ( $b_1$ )	$\tau_p, \tau_r$	The peak strength and the residual strength of the stress–strain curve ( $b_4$ )
$V_{\text{Quartz}}, V_{\text{Carbonate}}, V_{\text{Clay}}$	The contents of quartz, carbonate and clay, respectively ( $b_2$ )	$\varepsilon_r, \varepsilon_t$	The reversible strain and total strain of the stress–strain curve ( $b_5$ )
		$\varepsilon_p, \varepsilon_r$	The peak strain and residual strain of the stress–strain curve ( $b_6$ )
		$W_{ir}, W_e$	The irreversible strain energy before the peak and the elastic strain energy accumulated in the rock ( $b_7$ )
✉ Chi Ai aichi2017@163.com		$W_r, W_e$	The rupture energy after the peak and the elastic strain energy accumulated in the rock ( $b_8$ )
✉ Yu-wei Li liyuweibox@126.com		$B_C$	The brittleness index of coal established in this paper

<sup>1</sup> Department of Petroleum Engineering, Northeast Petroleum University, Daqing 163318, China

<sup>2</sup> Petrochina Research Institute of Petroleum Exploration and Development, Langfang 065006, China

<sup>3</sup> College of Automation, Harbin Engineering University, Harbin 150001, China

$B_{pre}$	The index for characterizing brittleness characteristics at the pre-peak stage ( $B_C$ )
$B_{post}$	The index for characterizing brittleness characteristics at the post-peak stage ( $B_C$ )
$B_I$	The anti-normalization of $B_C$
$\sigma_A$	The crack damage stress, or the yield stress of the stress–strain curve ( $B_C$ )
$\sigma_B, \sigma_C$	The peak strength and residual strength of the stress–strain curve ( $B_C$ )
$U_{pre}$	The total strain energy before peak point, <i>OABN</i> in Fig. 1 ( $B_C$ )
$U_d$	The dissipated strain energy before peak point, <i>OABM</i> in Fig. 1 ( $B_C$ )
$U_e$	The elastic strain energy before peak point, <i>MBN</i> in Fig. 1 ( $B_C$ )
$U_a$	The dissipated strain energy after peak point, <i>NBCE</i> in Fig. 1 ( $B_C$ )
$U_r$	The released strain energy used to maintain crack propagation after peak point, <i>MBCP</i> in Fig. 1 ( $B_C$ )
$U_{er}$	The residual strain energy of rock after its complete failure, <i>PCE</i> in Fig. 1 ( $B_C$ )
$E$	Elastic modulus of coal, the slope of <i>OA</i> in Fig. 1 ( $B_C$ )
$M$	Softening modulus of coal, the slope of <i>BC</i> in Fig. 1 ( $B_C$ )
$D$	Yield modulus of coal, the slope of <i>AB</i> in Fig. 1 ( $B_C$ )
$\sigma_3$	The confining pressure in triaxial compression tests
$\beta$	The inclined angle of face cleats in uniaxial compression tests

## 1 Introduction

Because of the ultra-low permeability of coalbed methane (CBM) reservoirs, the combination of horizontal drilling and multistage hydraulic fracturing technology is commonly used to enhance CBM production; however, field experiences reveal that not all hydraulic fracturing targets can yield on a commercial level (Wei et al. 2011; Soliman

et al. 2012; Zhang et al. 2017). Brittleness, an important mechanical index of coal, is closely related to the initiation and propagation of hydraulic fractures in CBM reservoirs, representing the ability of a reservoir to create a complex fracture network (Cipolla et al. 2010; Liu et al. 2012; Wu et al. 2013). The evaluation of hydraulic fracturing considering the coal brittleness index is important for efficient development and utilization of CBM resources (Wu et al. 2016; Li et al. 2017a, b, c). A scientific and practical index for evaluating coal brittleness can provide guidance when selecting fracturing targets and designing hydraulic fracturing projects in CBM reservoirs.

Many scholars have proposed different methods for evaluating rock brittleness based on their intended use. Honda and Sanada (1956), Lawn and Marshall (1979), Quinn and Quinn (1997), and Copur et al. (2003) used rock hardness properties to quantify rock brittleness by testing macro-indentation hardness and micro-indentation hardness. Protodyakonov (1963) and Blindheim and Bruland (1998) used the product of compressive strength and the percentage of fines to quantify rock brittleness based on the Protodyakonov impact test and UCS testing. Yagiz (2009) defined rock brittleness as the ratio of the maximum applied force to the corresponding penetration depth based on the punch test. While all these penetration, impact and hardness test approaches to rock brittleness were applied to evaluate drillability, they may not be appropriate for characterizing the hydraulic fracturing behavior of unconventional reservoirs because they do not consider the influence of loading conditions and rock anisotropies on brittleness (Holt et al. 2015; Kaunda and Asbury 2016).

At present, there are five main types of brittleness indices that can be applied in the field of unconventional oil and gas development. (1) Brittleness index based on the elastic parameters. Rickman (2008) proposed the brittleness index  $b_1$  based on field data of hydraulic fracturing at the Barnett shale reservoir ( $b_1 = YM\_BRIT + PR\_BRIT$ ). The results showed that the Elastic modulus ( $E$ ) and Poisson's ratio ( $\nu$ ) are the two major factors affecting the brittleness of shale. This approach, however, has two major limitations. First, this index is an empirical formula based on the field data, and the physical basis is insufficient. Second, the calculation results of this method are very sensitive because of the large dimensional difference between  $E$  and  $\nu$ . (2) Brittleness indices based on the contents of brittle minerals in the material. Jarvie (2007) showed a clear positive correlation between quartz content and rock brittleness ( $b_2 = V_{Quartz} / (V_{Quartz} + V_{Carbonate} + V_{Clay})$ ). However, this index neglects the influence of the stress state and diagenetic process on rock brittleness. Moreover, this method cannot be applied to evaluate the brittleness of CBM reservoirs because of the low content of inorganic minerals in coal. (3) Brittleness indices based on the strength parameters. Hucka and Das (1974)

characterized the rock brittleness by the ratio of its uniaxial compressive strength to tensile strength ( $b_3 = \sigma_c / \sigma_t$ ). Bishop (1967) established the brittleness index  $b_4$  based on the peak strength and the residual strength of rocks ( $b_4 = (\tau_p - \tau_r) / \tau_p$ ). (4) Brittleness indices based on the strain parameters. Hucka and Das (1974) proposed to use the reversible strain before rock failure to characterize the rock brittleness ( $b_5 = \varepsilon_r / \varepsilon_t$ ). Hajiabdolmajid and Kaiser (2003) defined the brittleness index  $b_6$  based on the post-peak strain characteristics after a series of rock mechanics tests ( $b_6 = (\varepsilon_p - \varepsilon_r) / \varepsilon_t$ ). The strength parameters can reflect the capacity of the rock to resist damage and failure, while the strain parameters can characterize the deformation characteristics of the rock before and after its failure. Brittleness is a comprehensive representation of the strength and strain characteristics during the rock failure process. In some cases, the calculated results of methods (3) and (4) are contradictory because of the isolated consideration of rock strength and deformation (Stavrogin and Tarasov 2001; Altindag 2003; Geng et al. 2016). (5) Brittleness index based on the strain energy. The evolution of strain energy during rock failure can reflect the characteristics of the process from crack initiation and growth to rock failure; thus, the brittleness index based on the strain energy can reflect the characteristics of the brittle rupture of rock better than other methods. Kidybinski (1981) suggested that the irreversible strain energy before rock failure was the key factor to characterize rock brittleness ( $b_7 = W_{ir} / W_e$ ). However, Tarasov and Potvin (2013) found that the rupture energy after rock failure was the decisive factor affecting rock brittleness ( $b_8 = W_r / W_e$ ). Brittleness is a comprehensive mechanical property of rock, which is correlated to both pre-peak and post-peak brittleness characteristics during the rock failure process. Therefore, accounting for only the pre-peak or the post-peak brittleness is inappropriate when establishing the brittleness index.

In view of the limitations of the existing rock brittleness indices and the urgent demand for an assessment parameter to help predict the hydraulic fracturing effect of CBM reservoirs, it is necessary to find a practical and reliable method to evaluate the brittleness of coal. The deformation and failure process of rock is accompanied by energy accumulation, energy dissipation and energy release, and the rock failure is essentially the structural instability driven by this energy. In this paper, the evolution of the strain energy at various stages of the coal failure process was analyzed based on the stress–strain curves. The main energy parameters influencing coal brittleness at the pre-peak stage and post-peak stage were determined. Based on this analysis, a new index for evaluating the brittleness of coal was established, which can comprehensively reflect the mechanical characteristics before and after coal failure. Uniaxial and triaxial compression tests of coal specimens monitored by an acoustic emission (AE) system were carried out. The brittleness of the

coal specimens under different confining pressures and cleat inclination angles were calculated by the new index, and the rationality and applicability of the new brittleness index were verified by the experimental results. This paper also presents analysis of the influences of the confining pressure and cleat direction on the stress–strain characteristics, the evolution of the strain energy and AE energy, the failure patterns and the brittleness of the coal.

## 2 Evaluation Method of Coal Brittleness Based on Energy Evolution

### 2.1 Energy Evolution During the Coal Failure Process

Rock failure is essentially a process that progresses from energy accumulation to energy dissipation and ends in energy release. The stress–strain curve is the external manifestation of the energy evolution during rock failure. The strain energy density is the accumulated strain energy per unit volume of rock material, that is, the area under the stress–strain curve. The strain energy evolution during the whole rock failure process can be divided into three stages (Fig. 1).

- I. *Energy accumulation—OA*. At this stage, the rock specimen undergoes mostly elastic deformation under the axial stress. The elastic strain energy density accumulated in stage (I) is the area of  $ODA$ .
- II. *Energy dissipation—AB*.  $\sigma_A$  represents the crack damage stress or the yield stress. At this stage, the pre-peak strain energy ( $U_{pre}$ ) produced by the external force transforms into reversible elastic strain energy ( $U_e$ ) and pre-peak dissipated energy ( $U_d$ ).
- III. *Energy release—BC*. This stage involves energy dissipation accompanied by a sudden release of strain energy. The post-peak dissipated strain energy ( $U_a$ ) results in further damage to the failed rock specimen, while the released strain energy ( $U_r$ ) is the rupture energy that drives the continuous propagation of macroscopic cracks.

There is a significant difference between the energy evolution of the brittle and plastic rock. In Fig. 2, the curves  $O_2A_2BC_2$  and  $O_1A_1BC_1$  represent the stress–strain curves of the brittle rock and the plastic rock, respectively. For a more intuitive comparative analysis, the peak strength ( $\sigma_B$ ) and the elastic modulus ( $E$ ) of these two curves are assumed to be equal, which means that the elastic strain energy accumulated in the brittle and plastic rock are the same. Nicksiar and Martin (2013), Zhao et al. (2015) and Cheng et al. (2016) studied the effects of the confining pressure on the crack damage

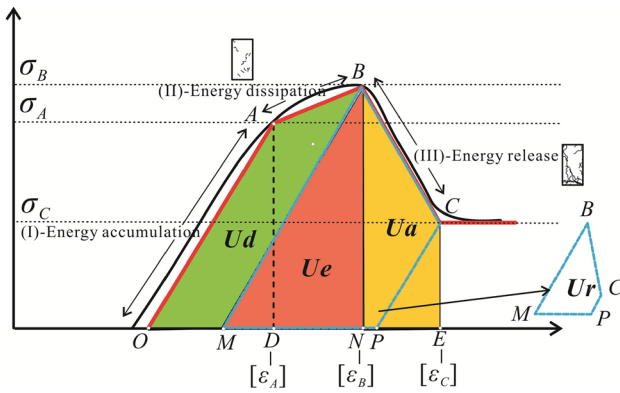


**Fig. 1** Strain energy evolution during the rock failure process

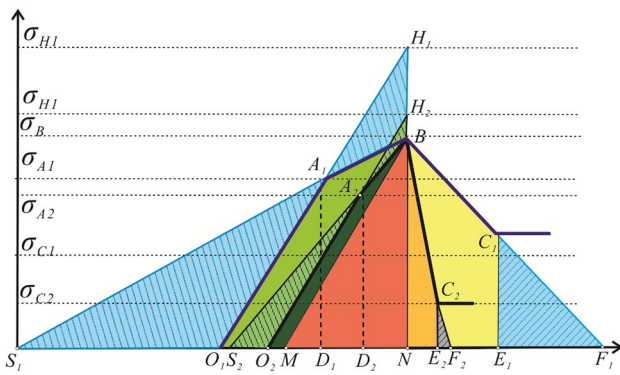


**Fig. 2** Comparison of energy evolution between brittle and plastic rock material. *MBN* elastic strain energy  $U_e$ ; *OABM* pre-peak dissipated energy  $U_d$ ; *OABN* total pre-peak strain energy  $U_{pre}$ ; *NBCE* post-peak dissipated strain energy  $U_a$ ; *NBCP* released strain energy  $U_r$ ; *PCE* residual elastic energy

stress through mechanical tests and rock constitutive modeling. Their results showed that the ratio  $\sigma_A/\sigma_B$  is positively correlated to the confining pressure, but negatively correlated to rock brittleness. Zhang and Gao (2015), Zuo et al. (2015) and Xia et al. (2017) proved that the velocity and amplitude drop in the post-peak stress of brittle rock was greater than that of plastic rock. This supports the relations shown in Fig. 1 between  $\sigma_{A1}$  and  $\sigma_{A2}$  and between  $\sigma_{C1}$  and  $\sigma_{C2}$ .

(a) At the pre-peak stage, the area of  $O_1A_1BC_1$  is larger than that of  $O_2A_2BC_2$ , which indicates that brittle rock has less pre-peak dissipated energy than plastic rock. The damage evolution of the plastic rock at the pre-peak stage is more obvious and is manifested in two aspects—time and degree. Chen et al. (2017) indicated that as the dissipated strain energy at the pre-peak stage decreased, the surface energy of the cracks increased, and the number and length of the macroscopic cracks in the rock specimen increased.

(b) Energy dissipation also occurs in the post-peak stage along with the release of strain energy. In Fig. 1, the area *MBCE* represents the total strain energy ( $U_{tot}$ ) accumulated inside the rock during the post-peak stage, which transforms into rupture energy ( $U_r$ ) and residual elastic energy ( $U_{er}$ ). The rupture energy maintains the propagation of the macroscopic cracks. Tarasov and Randolph (2016) showed that the elastic energy accumulated in the absolute brittle rock was sufficient to drive its entire rupture process, and the stress–strain curve of the absolute brittle rock dropped vertically at the post-peak stage. Zhang and Gao (2015) and Hou et al. (2016a, b) found that the drop of the post-peak stress–strain curve of brittle rock was rapid and large. Therefore,  $U_a$  represents the additional energy provided by the testing apparatus to maintain further damage of the rock specimen at the post-peak stage. For brittle rock, the post-peak dissipated energy is very small, and the energy release after the peak is very rapid (Rummel and Fairhurst 1970; Mishra and Nie 2013; Yang et al. 2016; Heng et al. 2015; Ai et al. 2016).

The elastic energy accumulated in the rock is the driving force for rock rupture. When the accumulated elastic energy is sufficient to maintain the rupture, the energy evolution during the failure process can reach a perfect balance and does not need additional external energy; this is the rupture characteristic of ideal brittle rock. From this point of view, the dissipated energy at the pre-peak stage weakens the accumulation of elastic energy, while the dissipated energy at the post-peak stage is added to the elastic energy. Thus,  $U_d$  and  $U_a$  have an essential connection with brittle rupture in rock.

### 2.2 Establishing the Coal Brittleness Evaluation Index

From the above analysis, it can be seen that the levels of the dissipated energy at the pre-peak and post-peak stages are the essential factors determining the brittleness of coal.  $U_e$ ,  $U_d$  and  $U_a$  can be calculated as follows (Xie et al. 2009; Huang and Li 2014; Peng et al. 2015; Meng et al. 2016; Xue et al. 2016; Li et al. 2017a, b, c):

$$U_e = AL \cdot \frac{\sigma_B^2}{2E}, \tag{1}$$

$$U_d = AL \cdot \left( \int_0^{\epsilon_B} \sigma_i d\epsilon_i - \frac{\sigma_B^2}{2E} \right), \tag{2}$$

$$U_a = AL \cdot \left( \int_{\epsilon_B}^{\epsilon_C} \sigma_i d\epsilon_i \right), \tag{3}$$

where  $A$  and  $L$  represent the cross-sectional area and height of the coal specimen, respectively, in mm;  $\sigma_i$  is a function of the stress–strain curve and  $\varepsilon_i$  is the strain; other symbols are as shown in Fig. 1.

To account for all the types of strain energy during the coal failure process, an integral of the stress–strain function is necessary, involving complex calculations. Moreover, the stress–strain curve of coal often fluctuates because of the development of cleats, and this can influence the calculation results. Therefore, an indirect approach is proposed in this paper to establish the brittleness evaluation index. In Fig. 2, the areas  $S_{\Delta SAO}$  and  $S_{\Delta ECF}$  are obtained by extending  $BA$  and  $BC$ , and the calculation formula of coal brittleness can be written as follows:

$$B_C = B_{pre} + B_{post} = \frac{S_{\Delta OAS}}{S_{\Delta MBN}} + \frac{S_{\Delta ECF}}{S_{\Delta MBN}} \tag{4}$$

In Figs. 1 and 2, the slopes of  $OA$  and  $BC$  represent the elastic modulus ( $E$ ) and the softening modulus ( $M$ ), respectively. For the convenience of calculation,  $AB$ —the slope of stage (II)—was defined as the yield modulus, denoted by  $D$  in this paper. Thus, Eq. (2) can be simplified as

$$B_C = \frac{S_{\Delta OAS}}{S_{\Delta MBN}} + \frac{S_{\Delta ECF}}{S_{\Delta MBN}} = \frac{\frac{\sigma_A^2}{2D} - \frac{\sigma_A^2}{2E}}{\frac{\sigma_B^2}{2E}} + \frac{\frac{\sigma_C^2}{-2M}}{\frac{\sigma_B^2}{2E}} = \frac{M\sigma_A^2(E - D) - DE\sigma_C^2}{DM\sigma_B^2} \tag{5}$$

Rock material can contain only a certain amount of accumulated energy and the surplus energy is released when the accumulated energy exceeds this limit. In Fig. 2,  $OABN$  represents the actual limit of the rock’s accumulated energy. When the stress exceeds the actual compressive strength ( $\sigma_B$ ), the accumulated energy reaches its limit and the destruction of the rock begins as it releases energy. Assuming that no damage occurred in the rock before its failure, the energy accumulated in the rock will reach the limit when the axial stress exceeds  $\sigma_H$ . Therefore,  $ABH$  indicates the loss of the rock’s capacity to accumulate the elastic energy because of the damage inside the rock material. The area of  $SAO$  is determined jointly by  $\sigma_A$ ,  $D$  and  $E$ ; thus,  $SAO$  indicates the ability of the rock material to dissipate energy before its failure. For the absolute brittle rock there is no plastic deformation stage or energy dissipation before the peak. In this case,  $ABH$  and  $SAO$  are close to 0. Therefore,  $ABH$  and  $SAO$  represent the loss of rock brittleness at the pre-peak stage of rock failure, and can reflect the ability of the rock to accumulate elastic strain energy.

After the failure of the rock, some residual elastic energy ( $PCE$  in Fig. 1) still remains in the rock because the rock does not completely lose its strength and integrity. The area of  $CEF$  represents the extra energy provided during the test, required for the release of all of the residual elastic energy. After the failure of the rock material with absolute

brittleness, all the energy is released, the rock is completely crushed and the residual elastic energy is 0. Therefore,  $CEF$  indicates the ability to release energy, and reflects the degree of rock fragmentation. The smaller the  $CEF$  area, the greater and faster the energy released after rock failure, and the larger the degree of fragmentation of the rock crushed. From the above analysis, it can be seen that, in the physical sense, the brittleness index  $B_C$  represents the ability of the rock to effectively accumulate the elastic energy before the peak and to violently release the post-peak energy, and also reflects the loss of rock brittleness before the peak and the degree of rock fragmentation after the peak.

To assess the brittleness of a set of coal specimens directly, the calculation results of Eq. (2) can be normalized as follows:

$$B_I = \frac{B_C - B_{Cmax}}{B_{Cmin} - B_{Cmax}} \tag{6}$$

where  $B_C$  and  $B_I$  are the evaluation indices of coal brittleness before and after normalization;  $B_{pre}$  and  $B_{post}$  describe the brittleness characteristics at the pre-peak and post-peak stages in Eq. (4), respectively; and  $B_{Cmax}$  and  $B_{Cmin}$  are the maximum and minimum calculated values of the brittleness index of the coal specimens.

$B_I$  is positively correlated to the coal brittleness, and its range is 0–1. Because of the overall consideration of the pre-peak and post-peak energy evolution during the failure process of coal,  $B_C$  and  $B_I$  have a firmer physical basis and can describe the brittleness characteristics better than other indices.

### 3 Tests on AE Energy Behavior of Coal Failure Under Different Conditions

#### 3.1 Characteristics of the Cleat System in Coal

The natural fractures in coal are often referred to as cleats, which can be classified as face cleats and butt cleats. Face cleats are continuous and are long, while butt cleats are discontinuous and develop between two sets of adjacent face cleats. Butt cleats are often perpendicular to the face cleats, and both are perpendicular to the bedding planes (Kulander et al. 1993; Jing et al. 2016; Mostaghimi et al. 2017; Busse et al. 2017). During the hydraulic fracturing of CBM reservoirs, the opening or shearing of cleats assists the formation of a complex fracture network. Therefore, the development characteristics of cleats should be considered in the brittleness evaluation of CBM reservoirs. The stress–strain curves represent the mechanical properties of coal under an external load. Therefore, the evolution of the strain energy obtained from the stress–strain curves can



reflect the effect of cleats on the mechanical properties and brittleness of coal (Kong et al. 2015; Feng 2017).

The coal samples studied in this paper were taken from the Jixi coal mine in Heilongjiang Province, China; the samples are mostly bright coal and contain some mirror coal seams. As shown in Fig. 3, the macroscopic distribution of the cleats is well-defined and uniform. Figure 4 shows a scanning electron microscope (SEM) image of cleats in a coal specimen. From both macroscopic and microscopic perspectives, we can see that the face cleats and butt cleats are interconnected and approximately perpendicular to each other. The density of the cleats, which refers to the number of cleats per 5 cm, is usually used to characterize the degree of development of the cleats in a coal specimen. The density of face cleats and butt cleats measured in the coal samples was 11.4–18.7 and 6.3–13.2, respectively.

### 3.2 Test procedures

Two groups of tests were carried out in this study. Group (1) was the uniaxial compression tests of coal under different inclination angles of face cleats. The aim of these tests

*NBCP* – released strain energy  $U_r$ ; *PCE* – residual elastic energy.

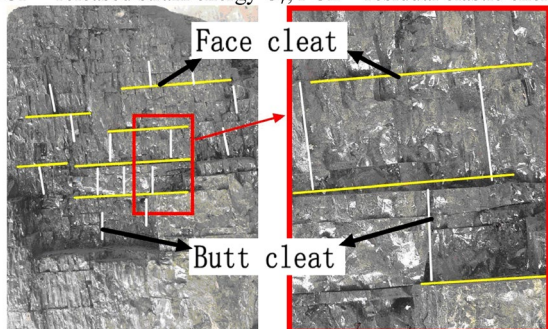


Fig. 3 Macroscopic distribution of cleats in coal

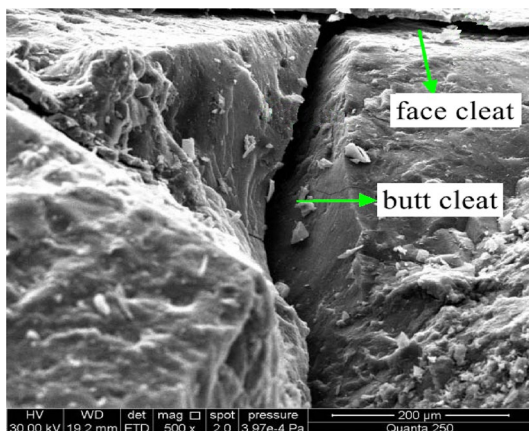


Fig. 4 SEM image of cleats in a coal specimen (500 $\times$ )

was to examine the effect of the direction of the cleats on the mechanical properties and brittleness of the coal. For brevity,  $\beta$  was used to represent the angle between the face cleats and the horizontal direction, that is, the inclination angle of the face cleats. Coal specimens with  $\beta$  values of 0°, 30°, 45°, 60° and 90° were tested. Group (2) was the triaxial compression tests of coal under different confining pressures and constant  $\beta$ . An MTS 815 electro-servo controlled testing system (MTS, Minnesota, USA) was used to carry out this group of tests, and the confining pressures were set to 0, 6, 12, 18, 24 and 30 MPa, respectively. The confining pressure was first loaded at a loading rate of 0.025 MPa/s. Then the axial pressure was loaded by displacement control at a loading rate of 0.02 mm/s until the coal specimen was destroyed.

Acoustic emission (AE) technology is a method for detecting the internal state and mechanical characteristics of materials using sound signals. Many studies have shown that it is feasible to assess the damage state and crack evolution inside rock materials by observing and analyzing AE energy signals (Li et al. 2017a, b, c; Liang et al. 2017). The acoustic wave generated during the coal failure in the uniaxial and triaxial compression tests was monitored by an AE testing system PCI-2. The resonant frequency and threshold value of the AE detector were set to 140 kHz and 30 dB, respectively. The impact time and signal acquisition interval were set to 100  $\mu$ s and 0.05 s, respectively. The voltage of the threshold value was adjusted to 1.0 V. Through the AE device, the AE signals received by the detector were further processed into AE parameters, such as AE count, AE count rate and AE energy. The AE detectors were installed inside the triaxial pressure chamber by refitting the test system, so that the signal acquisition system could receive more reliable AE signals. In this study, the AE energy was selected as the main parameter to analyze the rupture patterns of the coal specimens, calculated as

$$E_{AE} = \int_{t_i}^{t_j} V^2(t) dt / R, \quad (7)$$

where  $E_{AE}$  represents the AE energy;  $t_i$  and  $t_j$  are the start time and end time of the signal acquisition [ $\mu$ s];  $R$  is the internal resistance; and  $V(t)$  is the signal voltage [V].

## 4 Analysis of the Test Results

### 4.1 The Stress–Strain Curves of Coal

In the following analysis, we denote the confining pressure and the inclined angles of the face cleats as  $\sigma_3$  and  $\beta$ , respectively. Figures 5 and 6 are the stress–strain curves under different  $\sigma_3$  and  $\beta$ . At stage (I), the stress increases linearly with increasing strain, indicating that external stress causes

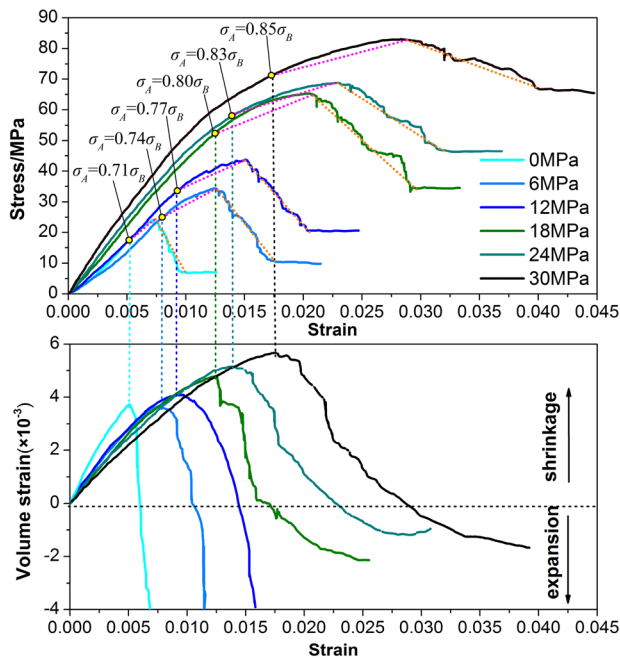


Fig. 5 The stress–strain curves of the coal specimens under different confining pressures ( $\sigma_3$ )

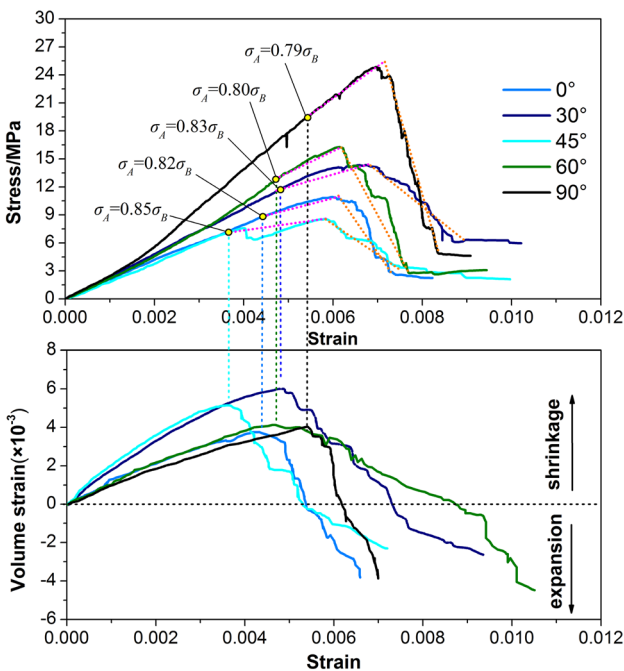


Fig. 6 The stress–strain curves of the coal specimens under different inclined angles of the face cleats ( $\beta$ )

elastic deformation of the coal specimen, but is not sufficient to drive the expansion of the existing micro-cracks and generate new micro-cracks. The original cracks inside

the coal specimen are in a relatively stable state, and the elastic strain energy accumulates continuously within the specimen. At the plastic deformation stage (II), the original micro-cracks inside the coal specimen gradually expand and new cracks are generated under the axial stress. Stage (II) is dominated by plastic deformation because of the evolution of the micro-cracks. The higher the plasticity of the coal specimen, the longer the plastic deformation stage in the stress–strain curve. At the post-peak failure stage (III), the cracks inside the coal specimen begin to expand rapidly, and macroscopic fracture surfaces can be observed on the coal specimens because of the convergence and the intersection of the micro-cracks. The expansion of the macro-cracks results in the structural failure of the coal, while the fragments of damaged coal specimens continue to slide along the fracture surfaces. This indicates that in stage (III) the coal undergoes continuous irreversible deformation as well as rapid structural destruction. The energy release process at this stage is accompanied by continuous dissipation of strain energy.

In Fig. 5, when the confining pressure is 0 MPa, stage (II) of the stress–strain curve is barely visible, and a large drop in both the velocity and amplitude of the stress occurs at the post-peak stage. When  $\sigma_3 = 12$  MPa, stage (II) is more significant, and the slope of the post-peak curve is smaller. When  $\sigma_3$  reaches 24 MPa, stage (II) of the curve extends over a very long duration and the stress drop at stage (III) is very slow, which reflects the strong plastic deformation characteristics.

In Fig. 6, the stress–strain curves and the peak strength of the coal specimens under different  $\beta$  are significantly different, which indicates that the direction of the cleats have a noticeable impact on the uniaxial compressive strength and brittleness of the coal. The uniaxial compressive strength of the coal decreases first and then increases as  $\beta$  changes from  $0^\circ$  to  $90^\circ$ . When  $\beta = 45^\circ$ ,  $\sigma_B$  of the coal specimen is at a minimum, and the plastic deformation and energy dissipation stage can be clearly observed in the stress–strain curve before the peak, reflecting the strong plastic characteristics of the coal specimen. When  $\beta = 90^\circ$ ,  $\sigma_B$  of the coal specimen reaches its maximum value. The plastic deformation stage is very short, and the post-peak stress drops rapidly and greatly, which shows obvious brittleness characteristics. However, when  $\beta = 30^\circ, 45^\circ$  and  $60^\circ$ , the specific relation between the coal brittleness and  $\beta$  cannot be directly determined from the stress–strain characteristics.

### 4.2 Analysis of Coal Brittleness

To further analyze the variation of coal brittleness with  $\sigma_3$  and  $\beta$ , Eqs. (5) and (6) were used to calculate the brittleness of the coal specimens. As shown in Fig. 7,  $B_{pre}$ ,  $B_{post}$  and  $B_C$  of the coal specimens gradually increase with increasing

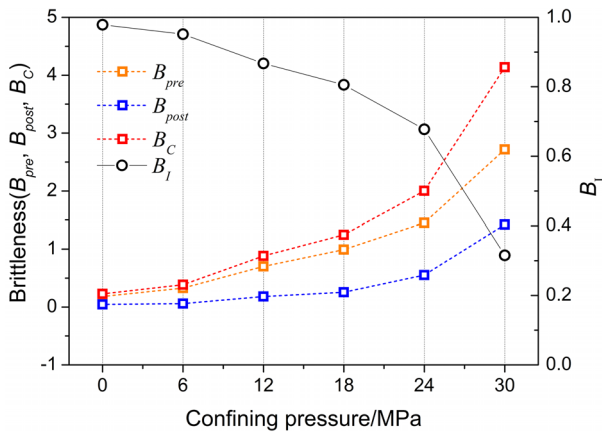


Fig. 7 Calculated results of coal brittleness under different  $\sigma_3$  values

confining pressure, indicating that the proportions of  $U_d$  and  $U_a$  in the total energy are positively correlated to the confining pressure level. The decrease of  $B_I$  with  $\sigma_3$  reflects the decrease in coal brittleness as the confining pressure increases. Figure 8 shows the numerical results of coal brittleness under different  $\beta$ . When the inclination angle of the face cleats increases from  $0^\circ$  to  $45^\circ$ ,  $B_I$  gradually decreases, indicating a decrease in the brittleness of the coal. When  $\beta = 45^\circ$ ,  $B_I$  (and the coal brittleness) decrease to their minimum value. However, when  $\beta > 45^\circ$ ,  $B_I$  begins to increase rapidly, and when  $\beta = 90^\circ$ ,  $B_I$  reaches its maximum value. The calculated brittleness of coal first increases and then decreases with the increase of the inclination angle of the face cleats; this is consistent with the analysis in Sect. 3.1. It is notable that when the face cleat angles are  $0^\circ$  and  $90^\circ$ , the results of  $B_{pre}$  and  $B_I$  under  $\beta = 0^\circ$  are different, but the  $B_{post}$  values are almost equal, which demonstrates that the coal specimens have the same pre-peak brittleness characteristics but different post-peak brittleness under these two angles.

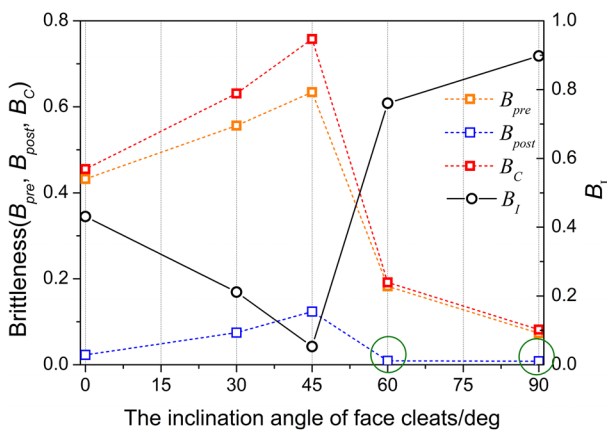


Fig. 8 Calculated results of coal brittleness under different  $\beta$  values

The pre-peak brittleness and post-peak brittleness of the coal are in complete agreement under different conditions.

For a further insight into the brittleness index, we compared  $B_I$  with other brittleness indices. The index  $b_2$  is based on the material’s mineral content and cannot reflect the influence of the confining pressure and anisotropy on rock brittleness.  $B_I$  is compared with other typical numerically derived brittleness indices in Fig. 9. The results of  $b_1$  show that the coal brittleness increases with increasing confining pressure, which is contrary to the results of other brittleness indices.  $b_1$  shows that the  $E$  and  $\nu$  have equivalent effects on rock brittleness, which does not agree with other findings and lacks sufficient physical basis (Guo et al. 2015; Chen et al. 2017). The brittleness indices  $b_4$  and  $b_6$  are based on the strength and strain, respectively. Although the overall trends of  $b_4$  and  $b_6$  decrease with increasing confining pressure, the rectangles (green dotted lines) in Fig. 9 mark notable data points;  $b_4$  under a confining pressure of 0 MPa is lower than that under 6 MPa, and  $b_6$  under a confining pressure of 18 MPa is lower than that under 24 MPa. Brittle rupture of rock is a phenomenon of dynamic instability driven by elastic strain energy, and the energy accumulation and release is determined by the strength and strain of the rock. It is inappropriate to characterize rock brittleness only on the basis of the strength or the strain parameters. In some cases, strength-based and strain-based brittleness indices cannot reflect the true variation of rock brittleness with changing stress and may result in conflicting results.

In Fig. 10,  $B_I$  is compared with the energy-based brittleness indices ( $b_7 = W_{ir}/W_e$  and  $b_8 = W_r/W_e$ ). When the confining pressure increases from 0 MPa to 6 MPa,  $b_7$  decreases as the confining pressure increases, but  $b_8$  remains almost constant. However, when the confining pressure increases from 12 MPa to 18 MPa,  $b_8$  decreases with increasing confining pressure and  $b_7$  maintains an almost constant value. In

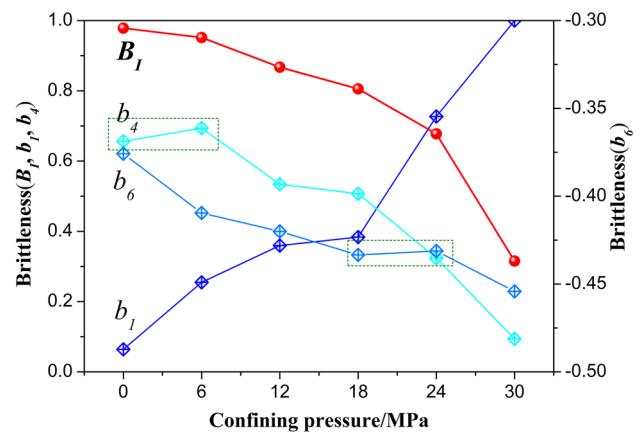


Fig. 9 Comparison of  $B_I$  and other typical brittleness indices ( $b_1$ —index based on elastic parameters,  $b_4$ —index based on strength parameters,  $b_6$ —index based on strain parameters)



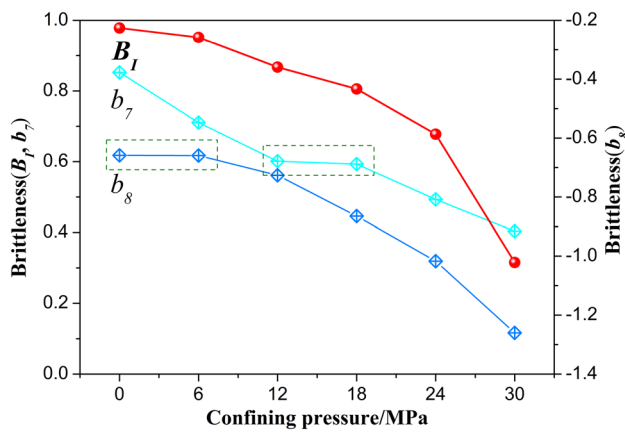


Fig. 10 Comparison of  $B_1$  and energy-based brittleness indices

the  $b_7$  curves, the effect of the post-peak energy on the rock brittleness is ignored and the  $b_8$  indicates that brittleness is only related to the post-peak rupture energy. Thus,  $b_7$  and  $b_8$  can only characterize the brittleness characteristics before or after the peak, respectively. The strain energy before the peak reflects the ability of the rock to accumulate energy, and the post-peak strain energy represents the characteristics of the released energy. Characterizing the rock brittleness solely based on the evolution of the energy either before or after the peak may limit the outcome, leading to conflicting results. Unlike other brittleness indices,  $B_1$  not only considers the comprehensive effect of the external loading conditions and the internal cleat system on the rock brittleness, but can also describe the brittleness characteristics before and after the peak, based on a solid physical basis and offering an easy and reliable calculation process.

### 4.3 Analysis of Strain Energy and AE Energy Characteristics

#### 4.3.1 Evolution Characteristics of the Strain Energy

The experimentally derived  $U_e$ ,  $U_d$  and  $U_a$  measured during the failure process of the coal specimens are presented in Table 1. In Fig. 11,  $U_e$ ,  $U_d$  and  $U_a$  increase gradually with  $\sigma_3$  because the confining pressure enhances the bearing capacity of the coal specimens. The energy ratios  $U_d/U_e$  and  $U_a/U_e$  are also positively correlated to  $\sigma_3$ , which indicates that the pre-peak and post-peak dissipated energy increases with  $\sigma_3$  under a prerequisite that the same elastic strain energy accumulates in the coal specimens. Under triaxial compression, the brittleness characteristics of the coal reflected by the strain energy are consistent with the calculated coal brittleness in Fig. 9. In Fig. 12, the strain energy of the coal specimens is plotted for different  $\beta$  values, showing different trends of  $U_e$ ,  $U_d$  and  $U_a$  compared with those of Fig. 11. The accumulated elastic strain energy and the post-peak dissipated strain energy reach their maximum values when  $\beta=90^\circ$ , but the pre-peak dissipated strain energy falls to its minimum value when  $\beta=30^\circ$ . The rupture of coal is a structural instability phenomenon driven by energy. The mechanical properties of the coal under uniaxial loading are significantly affected by the internal cleats, resulting in the different changes of the various energies required for the complete failure of the coal. Therefore, the change of a single strain energy cannot reflect the brittleness characteristics of coal. However, the ratios  $U_d/U_e$  and  $U_a/U_e$  represent the magnitudes of the pre-peak and post-peak dissipated energy relative to the elastic energy, respectively. Although the changes of these two ratios with  $\beta$  are not exactly the same, they agree with the calculated coal brittleness in Fig. 10, which indicates that the brittleness index indirectly

Table 1 Calculated results of strain energy density

Condition	Yield strength- $\sigma_A$ (MPa)	Peak strength- $\sigma_B$ (MPa)	Residual strength- $\sigma_C$ (MPa)	Elastic modulus $E$ (GPa)	Dissipated strain energy density at pre-peak stage, $U_d/V$ (MJ/mm <sup>3</sup> )	Elastic strain energy density $U_e/V$ , (MJ/mm <sup>3</sup> )	Dissipated strain energy density at post-peak stage, $U_d/V$ (MJ/mm <sup>3</sup> )	
$\sigma_3$ (MPa)	0	17.03	23.99	7.251	3.13	0.021	0.119	0.077
	6	25.41	34.33	10.51	3.31	0.105	0.259	0.171
	12	33.68	43.74	20.39	3.77	0.256	0.386	0.280
	18	51.93	64.92	34.01	3.91	0.537	0.728	0.629
	24	56.81	68.44	46.25	4.35	0.833	0.811	0.825
	30	75.02	80.03	72.51	4.51	1.602	1.085	1.367
$\beta$ ( $^\circ$ )	0	8.86	10.81	3.06	2.33	0.014	0.035	0.019
	30	11.83	14.26	6.16	2.42	0.023	0.034	0.023
	45	7.26	8.54	3.62	1.86	0.018	0.021	0.018
	60	12.97	16.22	3.15	2.99	0.011	0.048	0.024
	90	19.54	24.75	4.75	3.51	0.012	0.091	0.032

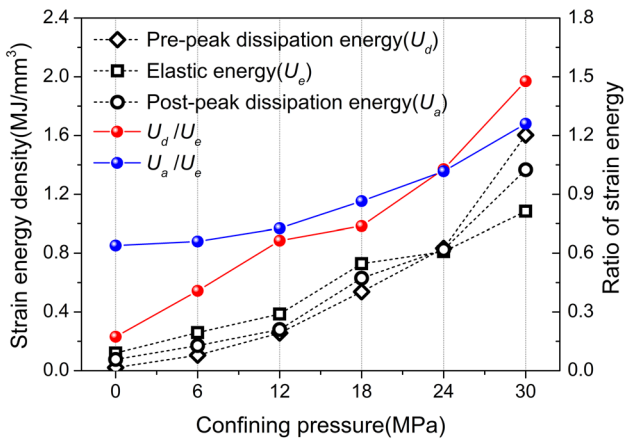


Fig. 11 Strain energy density and strain energy ratio under different  $\sigma_3$  values

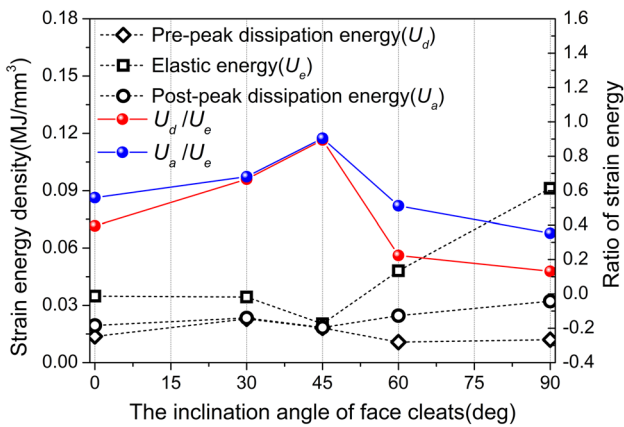


Fig. 12 Strain energy density and strain energy ratio under different  $\beta$  values

established by the areas of  $S_{\Delta SAO}$  and  $S_{\Delta ECF}$  (Fig. 2) is a reliable indicator that reflects the evolution of the strain energy and brittleness of coal.

### 4.3.2 Evolution characteristics of AE energy

Figures 13 and 14 are the AE energy–strain curves of the coal specimens under different conditions. The confining pressure and the inclined angle of the face cleats have a significant influence on the patterns of the AE energy–strain curves. According to the characteristics of the AE energy–strain curves and the corresponding stress–strain curves, the evolution of the AE energy during coal failure can be divided into three types, which are defined here as *Rapid Fracture Type*, *Plastic Fracture Type* and *Stable Fracture Type*.

1. *Rapid fracture type*. The AE energy–strain curves under the conditions of  $\sigma_3=0$  MPa and  $\beta=90^\circ$  are typical representatives of this type (Figs. 13a, 14c). The stress–strain curves of this type exhibit linear elastic deformation in stage-(I) and barely visible plastic deformation in stage (II) before the peak, and a rapid and great stress drop at the post-peak stage. When the axial stress is less than  $\sigma_A$ , the AE phenomena are not significant and the AE energy is low. The AE energy gradually increases when the stress exceeds  $\sigma_A$ , and then increases rapidly to its peak value when the axial stress approaches  $\sigma_B$ . At the post-peak stage (III), the AE energy drops rapidly and remains at relatively low values. Figures 15 and 16 show the accumulated AE energy–time curves under different conditions. Taking the curve under the confining pressure of 0 MPa as an example, the increase of the accumulated AE energy is very slow at stages (I) and (III), but quite rapid at stage (II). The accumulated AE energy–time curve of the *Rapid Fracture Type* has approximately linear lower and upper sections, with a very rapid rise between them, which indicates that the accumulation rate of the AE energy has a sudden change at the points corresponding to  $\sigma_A$  and  $\sigma_B$ . The *Rapid Fracture Type* curves represent coal with strong brittleness characteristics.

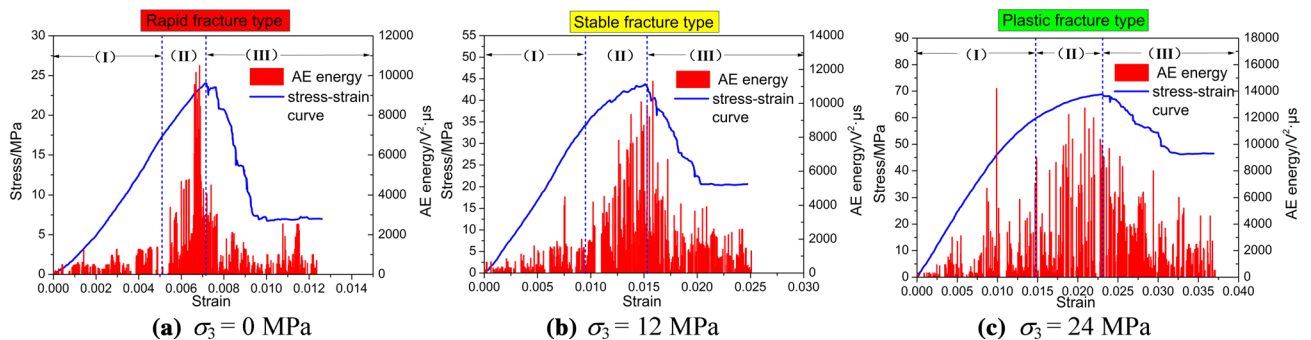


Fig. 13 AE energy–strain curves of coal specimens under different  $\sigma_3$  values

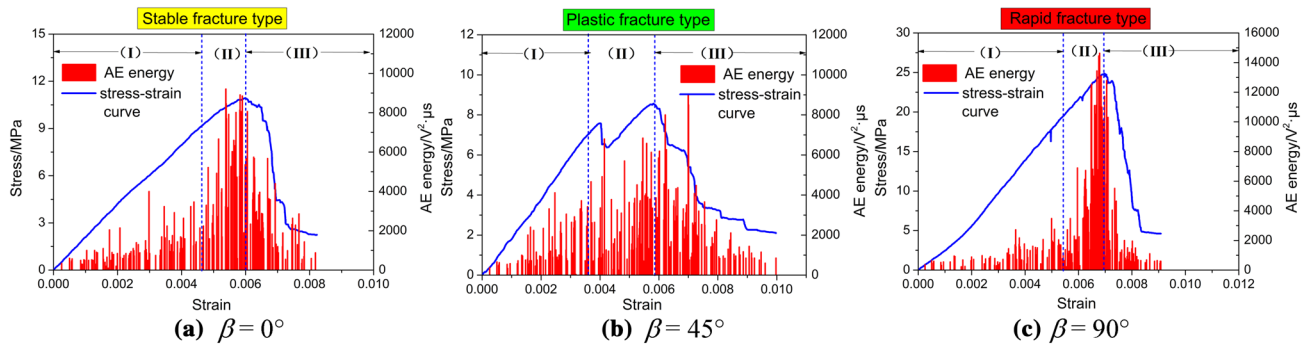


Fig. 14 AE energy-strain curves of coal specimens under different  $\beta$  values

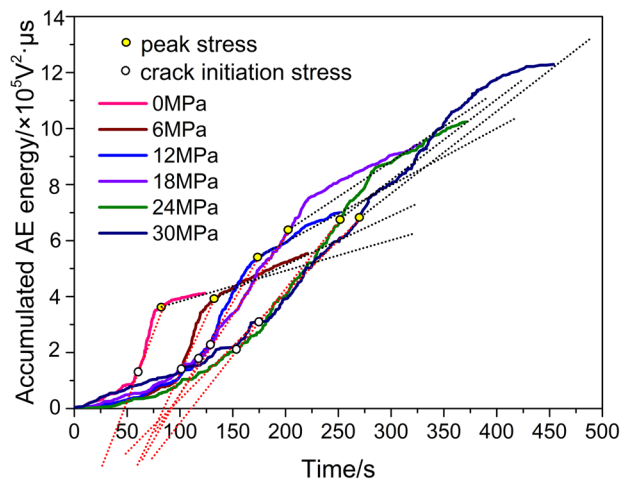
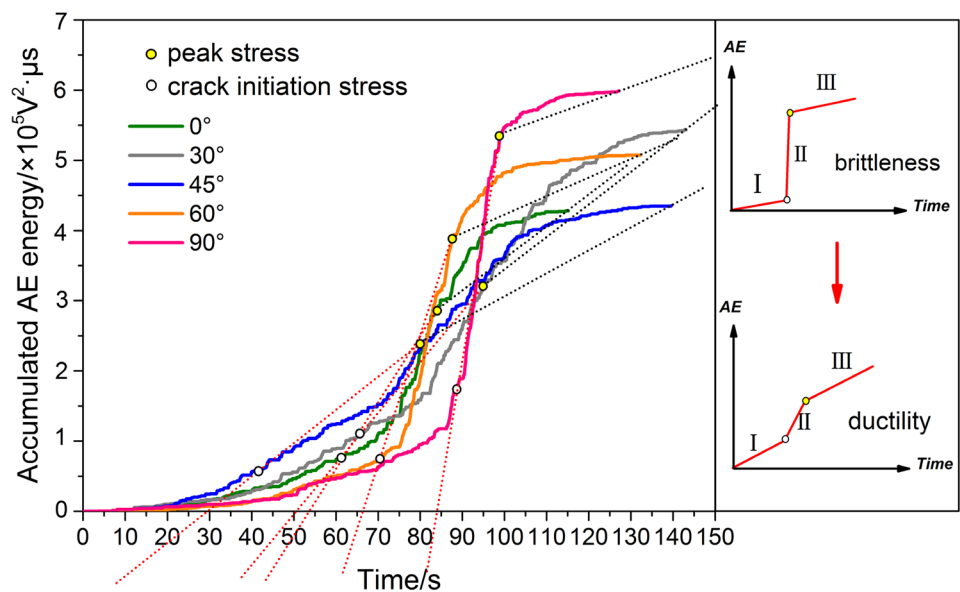


Fig. 15 Accumulated AE energy-time curves of the coal specimens under different  $\sigma_3$  values

2. *Plastic fracture type.* This type is typically represented by the AE energy-strain curves under the conditions of  $\sigma_3 = 24$  MPa and  $\beta = 45^\circ$  in Figs. 13c and 14b. The stress-strain curves of this type show very pronounced plastic deformation in stage (II) before the peak, and a slow decrease of stress at the post-peak stage (III). For the AE energy-strain curves of this type, the AE energy begins to increase at stage (I), then it decreases slowly and remains relatively high during stage (III). Generally, in this type of curve the AE energy has more than one peak during the failure process, with considerable separation between the peaks. The peak value of the AE energy in Fig. 13c is at stage (I), while the peak in Fig. 14b is at the post-peak stage. In Figs. 15 and 16, the accumulated AE energy-time curves corresponding to the *Plastic Fracture Type* are first concave and then con-

Fig. 16 Accumulated AE energy-time curves of the coal specimens under different  $\beta$  values



vex, and have a gentle increase without sudden changes, which is characteristic of strong plastic deformation.

3. *Stable fracture type*. This type is represented by the curves in Figs. 13b and 14a, which show the transition between the *Rapid Fracture Type* and *Plastic Fracture Type*. Compared with the curves of the *Rapid Fracture Type*, these curves have a more obvious plastic yielding stage (II) and more pronounced AE characteristics at stage (I). Compared with the *Plastic Fracture Type*, however, the stress in these type of curves increases faster at stage (II) and the AE energy values at stage (I) and (III) are smaller.

In summary, the AE energy–strain curves and the accumulated AE energy–time curves transform from *Rapid Fracture Type* into *Stable Fracture Type* when the confining pressure increases from 0 to 18 MPa. The AE energy curve shows *Plastic Fracture Type* characteristics when  $\sigma_3$  reaches 24 MPa, indicating that the brittleness of the coal decreases gradually as the confining pressure increases, and the coal specimens show obvious plastic characteristics when the confining pressure increases to a certain level. For the coal specimens under different face cleat inclination angles, the AE energy curves were of the *Rapid Fracture Type* for  $\beta=90^\circ$  and showed characteristics of *Plastic Fracture Type* when  $\beta$  was  $45^\circ$  and  $30^\circ$ . In addition, for  $\beta=60^\circ$ , parts of the AE curves had characteristics of *Stable Fracture Type* while the others were of the *Rapid Fracture Type*. The brittleness characteristics reflected by the evolution of the AE energy under different conditions are consistent with the calculated brittleness based on the indices  $B_C$  and  $B_I$  in Sect. 3.2.

#### 4.4 Failure Patterns of the Coal Specimens

The failure patterns of the coal specimens under different confining pressures are shown in Fig. 17. The main feature is the multiple longitudinal splitting failure pattern accompanied by local shear failure when  $\sigma_3=0$  MPa. In addition, some specimens have a multiple Y-shaped rupture pattern because some adjacent splitting cracks were connected by a number of shorter shear cracks. When  $\sigma_3=6$  MPa, although the number of splitting cracks decreases, the dominant failure pattern does not change. When  $\sigma_3$  approaches 12 MPa, only longitudinal cracks can be observed on the coal specimens, with very few Y-shaped ruptures. When  $\sigma_3=24$  MPa, the failure patterns of the coal specimens change to shear failure accompanied by a few short longitudinal splitting cracks. When  $\sigma_3=30$  MPa, the coal specimens are dominated by pure shear failure, and most specimens only have one shear crack. In summary, the failure pattern of the coal specimens changed from multiple splitting failure to pure shear failure as the confining pressure increased. The reason for this change is that the confining pressure restricts

the propagation and coalescence of longitudinal cracks, and is beneficial to the expansion of the inclined cracks which are at an angle to the direction of the maximum principal stress. The longitudinal splitting crack is a type of tensile crack, which is easily opened and has a small displacement between the crack surfaces. Therefore, the dissipated energy needed to initiate and propagate the longitudinal splitting cracks is small. However, coal fragments will slide along the fracture surfaces after the shear failure of the coal specimen under a high confining pressure. This process requires the testing apparatus to provide more energy to overcome the friction and maintain the propagation of the macro-cracks. The failure patterns of the coal under different  $\sigma_3$  indicate that the brittleness and the ability to form complex fractures in coal decrease with increasing confining pressure.

Figure 17 also shows the failure patterns of the coal specimens under different inclination angles of the face cleats. When  $\beta=0^\circ$ , the coal specimens are dominated by the longitudinal splitting failure, and the longitudinal cracks are mostly split along the face cleats. Because the face cleats are parallel to the loading direction and have low cohesion, they open easily, forming tensile cracks. When  $\beta=30^\circ$  and  $45^\circ$ , the coal specimens shear along the face cleats. At the pre-peak stage, because the directions of face cleats and the maximum principal stress are close, the face cleats easily lose cohesion and form many slipped micro-cracks under the rising axial pressure. This process requires a large amount of energy to be dissipated. At the post-peak stage, the coal fragments continue to slip along the surfaces of the opened face cleats, and dissipate a large amount of energy because of the large contact area and friction forces between the surfaces.

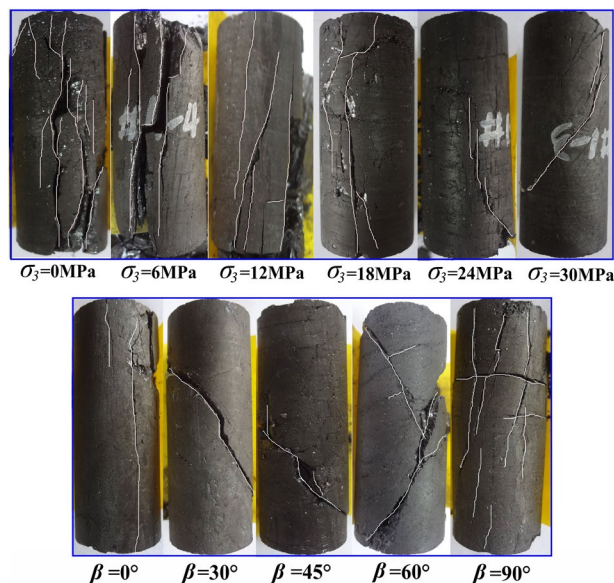


Fig. 17 Failure patterns of coal specimens under different  $\sigma_3$  and  $\beta$



Therefore, the accumulation rate of the AE energy at stage (II) is relatively small because the pre-peak-dissipated energy weakens the accumulated elastic energy, while the accumulation rate at stage (III) is relatively large because of the additional post-peak-dissipated energy. The corresponding stress–strain curve features relatively small  $D$  and  $M$  values. When  $\beta = 30^\circ$ , the coal specimens are dominated by the shear splitting mixed failure pattern. At the pre-peak stage, the micro-cracks open and slide along the direction of the butt cleats, which requires some dissipated energy. When the axial stress exceeds the peak strength, the opened micro-cracks continuously expand as the elastic energy is released. Because the butt cleats are discontinuous joints, the opened butt cleats may expand along the coal matrix or connect to other butt cleats nearby; this process leads to the formation of the shear splitting mixed failure patterns or the Y-shaped rupture cracks. However, when  $\beta = 60^\circ$ , the failure patterns of the coal specimens involve many types of macro-cracks, such as longitudinal splitting cracks, secondary shear cracks and cracks that open along the cleats. The face cleats do not easily open or shear under the action of axial stress because of the large angle between the face cleats and the loading direction. Combining the corresponding stress–strain curves, we conclude that only a small amount of dissipated energy is needed to drive the propagation of micro-cracks at the pre-peak stage, and the elastic energy rapidly accumulates in the coal specimen with increasing axial stress. When the axial stress exceeds the peak strength, the accumulation of energy reaches its limit, and the instantaneous release of large amounts of elastic energy requires more cracks to provide release paths. Furthermore, the failure pattern of the coal specimen is more complex because of the discontinuity of the butt cleats. The rapid formation of various types of cracks results in the rapid failure of the coal specimens and a small amount of dissipated energy after the peak. Therefore, the accumulated AE energy has a sudden change at points  $\sigma_A$  and  $\sigma_B$  and the stress–strain curves have relatively large  $D$  and  $M$  values.

Many scholars have studied the influence of joints on the failure patterns and acoustic emission characteristics of rock. However, most of these studies investigated only horizontally and vertically oriented joints (Qiao et al. 2015; Xu et al. 2017; Wang et al. 2017). Wasantha et al. (2014, 2015) systematically studied the influence of joint orientation on the failure patterns and AE characteristics of jointed sandstone. In their experiments, the failure patterns for specimens with joints having inclination angles of  $0^\circ$  and  $90^\circ$  were different from those of the coal specimens in this paper. When the inclination angle of the joint is  $0^\circ$ , the failure of the specimen mainly occurs by shearing through the material, which is similar to the behavior of intact rock. When the joint inclination angle is  $90^\circ$ , the failure patterns are dominated by longitudinal splitting failure patterns. This is because the

coal specimen has not only face cleats but also butt cleats which are perpendicular to the face cleats. The butt cleats make the failure patterns of the coal specimens more complex. The failure mechanism for the specimens with joints inclined at  $30^\circ$  and  $45^\circ$  showed shear failure along the joints, similar to the experimental results of this paper.

Figure 18 shows the cumulative AE counts ratio vs. time from the singly jointed rock specimens in study of Wasantha et al. (2015). With joint inclination angles of  $0^\circ$  and  $30^\circ$ , the AE events tend to increase steadily as the axial load increases, similar to the AE curve of the coal specimen of the *Stable Fracture Type* in this paper. However, at stages (I) and (II), the coal specimens had more AE events than the singly jointed rock specimens. This can be attributed to the butt cleats, which intensify the internal damage before the failure of the coal specimen. When  $\beta = 45^\circ$ , many significant AE events appear at the beginning of the loading and throughout the whole loading process. The cumulative AE events showed steady linear growth, similar to that of the *Plastic Fracture Type* of this paper. In this case, both the coal and the singly jointed rock specimens are dominated by shear failure along the face cleats or joints, and the butt cleats have no effect on the failure pattern and AE characteristics. When  $\beta = 90^\circ$ , there are almost no AE events at the beginning of the loading. Many significant AE events appear suddenly until the axial load reaches a certain level and the cumulative AE curve increases sharply, indicating a brittle failure pattern and the rapid release of strain energy. Although the AE characteristics under an inclination angle of  $90^\circ$  are similar to the *Rapid Fracture Type* in this paper, the coal specimen has more AE events at the beginning of the loading than the singly jointed rock specimen because of the existence of butt cleats. In general, compared with the singly jointed rock, the failure patterns of coal are more

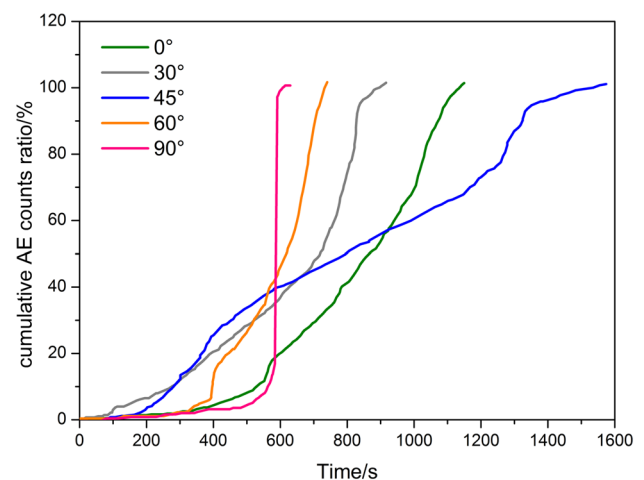


**Fig. 18** Cumulative AE counts ratio with time of the singly jointed rock specimens (Wasantha et al. 2015)

diversified and the acoustic emission responses are more significant than in the singly jointed rock because of the existence of the butt cleats.

### 4.5 Correlation Between the Mechanical Properties and Brittleness of Coal

Figure 19 shows the correlation between the strength characteristics and brittleness of coal specimens under triaxial loading. Under different confining pressures, the brittleness of the coal is negatively correlated to  $\sigma_A$ ,  $\sigma_B$  and  $\sigma_C$ , and has the best correlation with  $\sigma_C$  ( $R^2=0.9227$ ) and worst correlation with  $\sigma_B$  ( $R^2=0.7104$ ). In addition, the coal brittleness has good negative correlations with the ratios  $\sigma_A/\sigma_B$  and  $\sigma_C/\sigma_B$ . Under uniaxial loading with different  $\beta$  (Fig. 20), although the coal brittleness is negatively correlated with  $\sigma_A/\sigma_B$  and  $\sigma_C/\sigma_B$ , it has a poor positive correlation with  $\sigma_A$ ,  $\sigma_B$  and  $\sigma_C$  ( $R^2=0.31-0.55$ ). This indicates that the relations between the brittleness and strength of coal vary under different loading conditions, but the coal brittleness always increases with the strength ratios of  $\sigma_A/\sigma_B$  and  $\sigma_C/\sigma_B$ . The confining pressure can enhance the bearing capacity of coal specimens but will limit crack propagation and weaken the brittleness of coal, hence the negative correlation between the strength and brittleness of the coal specimens. Under the same confining pressure, the peak strength determines the level of elastic strain energy that accumulates in the specimen, while the elastic strain energy determines the level of the post-peak energy release. Therefore, coal specimens which have strong brittleness and are characterized by high energy accumulation and release also have large  $\sigma_A$ ,  $\sigma_B$  and  $\sigma_C$  values. Thus, the correlation between coal strength and

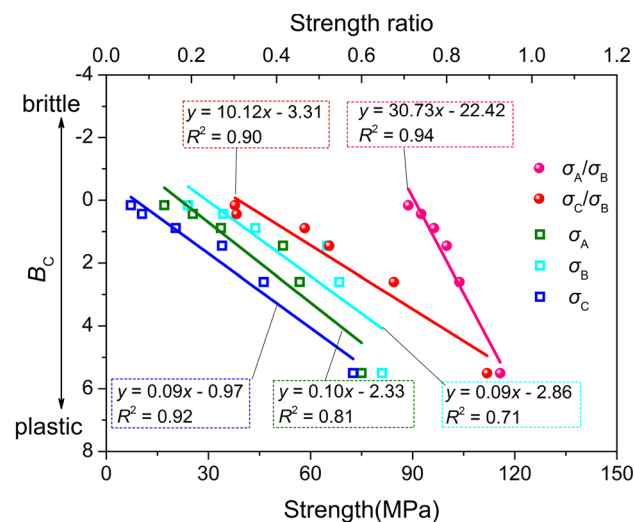


Fig. 19 Correlation between the strength and brittleness of coal under different  $\sigma_3$  values

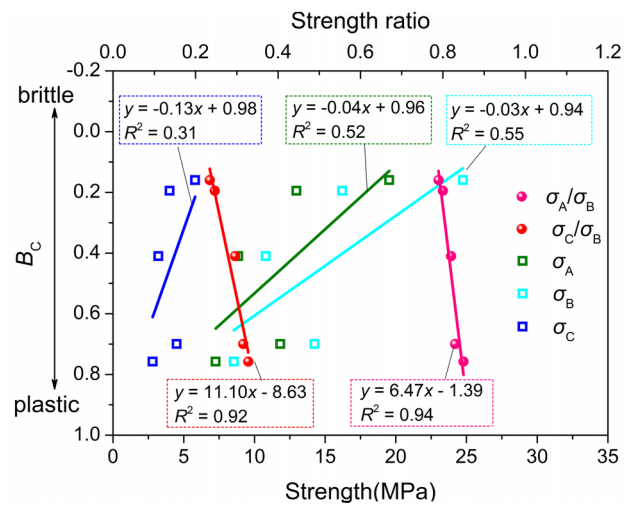


Fig. 20 Correlation between the strength and brittleness of coal under different  $\beta$  values

brittleness is positive but not very good because of the weakening effect of the cleats on the coal strength.

Figures 21 and 22 show the correlations between the coal brittleness and various moduli. Under uniaxial and triaxial loading both  $D$  and  $M$  have good positive correlations with the coal brittleness; however, the correlation between  $E$  and the coal brittleness is negative under triaxial loading but positive under uniaxial loading. The accumulation of the elastic energy depends on increased confining pressure under triaxial loading, but is only related to the mechanical properties of the coal under uniaxial loading; the large elastic modulus is the external manifestation of the rapid accumulation of elastic energy. Previous studies showed that the brittleness

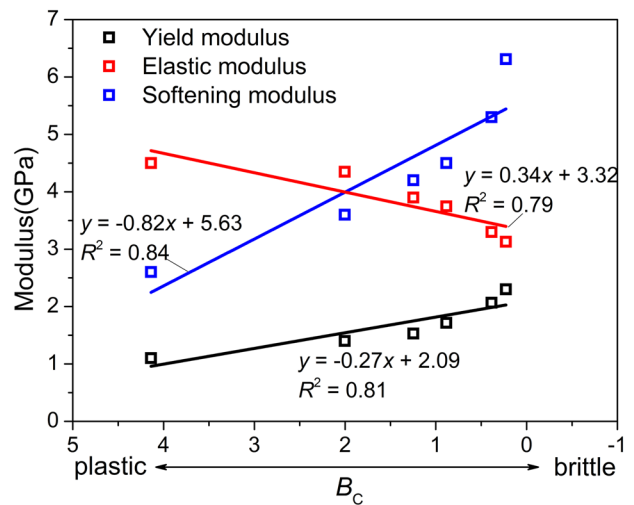


Fig. 21 Correlation between the modulus and brittleness of coal under different  $\sigma_3$  values

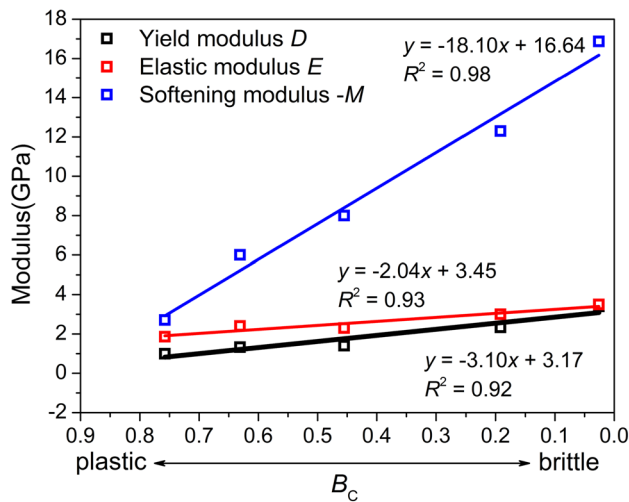


Fig. 22 Correlation between the modulus and brittleness of coal under different  $\beta$  values

of rock material always increases as E rises (Meng et al. 2015; Guo et al. 2015; Liu and Sun 2015); this conclusion is different from the relation observed in our study because these studies neglected the influence of the external stress state on the rock brittleness. Thus, the positive correlation between E and the brittleness of the rock is valid only under specific loading conditions.

Figures 23 and 24 show the correlations between the brittleness and the strain energy characteristics of the coal specimens. Under triaxial stress, the coal brittleness is negatively correlated with  $U_d$ ,  $U_e$  and  $U_a$  as well as with the energy ratios  $U_d/U_e$  and  $U_a/U_e$ , all exhibiting strong correlations ( $R^2 = 0.86-0.96$ ). The coal brittleness

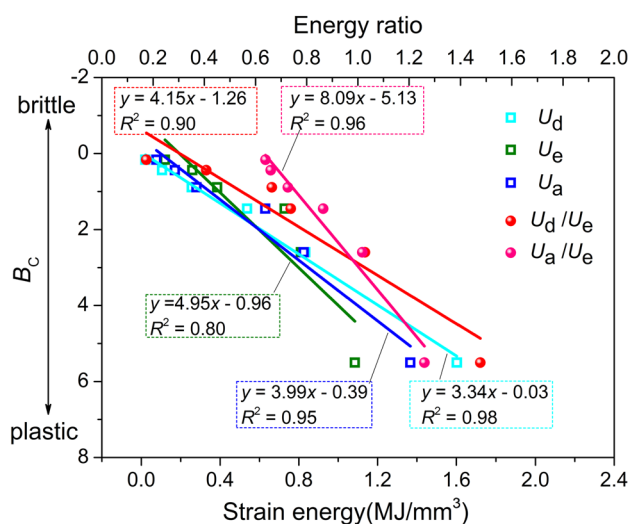


Fig. 23 Correlation between the strain energies and brittleness of coal under different  $\sigma_3$  values

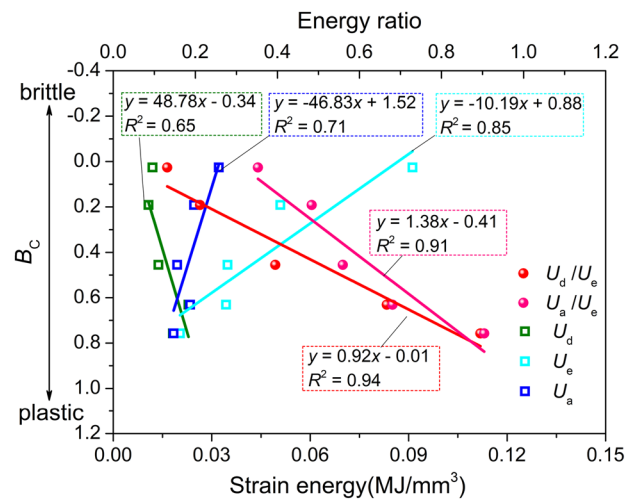


Fig. 24 Correlation between the strain energies and brittleness of coal under different  $\beta$  values

is positively correlated only with the elastic energy  $U_e$  under uniaxial loading, and has no clear relations with  $U_d$  and  $U_a$ ; however, the ratios  $U_d/U_e$  and  $U_a/U_e$  have a strong negative correlation with coal brittleness. This is consistent with the analysis in Sect. 4.3.1. The elastic strain energy is the driving force for the damage and rupture of coal, and the dissipated energy before and after the peak can characterize the coal brittleness only under the same accumulation of elastic strain energy.  $U_d/U_e$  and  $U_a/U_e$  have different correlations with the coal brittleness, which indicates once again that using only the pre-peak or the post-peak brittleness characteristics to derive the brittleness index will yield inaccurate results.

## 5 Discussion

Brittleness is an important basic property of rock and rock-like materials, which has been investigated by many scholars in different fields. However, different disciplines have different understanding of rock brittleness, therefore, currently there is no widely accepted brittleness definition or standard brittleness calculation method. Morley (1944) and Hetényi (1950) defined brittleness as the lack of ductility of the material. Howell (1960) proposed a concept of rock brittleness in which rock material ruptures or fractures with little or no plastic flow. Obert and Duvall (1967) described brittleness as a property of rock material that fractures rapidly at or slightly beyond the yield stress. According to the study of Tarasov and Potvin (2013), rock brittleness was defined as the ability of rock to self-sustain the failure process. From the rock mechanics aspect, brittleness can be described as the ability of rock material to deform continuously without

permanent deformation under stress which surpasses the stress limit corresponding to rock micro-cracking. It can be seen that the rock brittleness involves the damage characteristics (plastic deformation) before the failure and the rupture behavior after the failure. From the aspect of energy evolution, rock rupture is essentially the release of strain energy. If the energy accumulated in the rock before its failure is large enough, more cracks are needed to release the energy after the failure. Therefore, the brittle rupture of rock is associated with the characteristics of both the accumulation and the release of energy, which correspond to the damage characteristics before the failure and the rupture behavior after the failure. Energy dissipation before and after rock failure is the key factor in determining the accumulation and release of the strain energy (Labuz and Biolzi 1991; Mitri et al. 1999). Energy dissipation before the peak will weaken the effective accumulation of elastic energy. In laboratory experiments, to maintain the post-peak rupture the rock needs additional energy provided by the testing apparatus, which represents the dissipated energy after the peak. The physical meaning of the brittleness index derived in this study can be characterized as the ability of the rock material to effectively accumulate elastic energy at the pre-peak stage and to fully rupture, induced by the violent release of elastic energy, at the post-peak stage; these two processes reflect the loss of rock brittleness before the peak and the degree of rock fragmentation after the failure, respectively. If the accumulation of elastic energy is insufficient, brittle rupture of the rock will not occur. Even if the rock can accumulate a large amount of elastic energy, brittle rupture cannot occur if the rock lacks the ability to release the energy.

The brittleness index based on energy evolution can better reflect the brittleness characteristics during the rupture and failure process of coal. The brittleness index established in this paper can provide a reliable experimental method for evaluating coal brittleness; however, at present it is only suitable for evaluating the relative brittleness of coal under specific loading conditions because of the difference between the stress conditions during the tests and those in a real reservoir. Whether the brittleness index can be used as a general index for evaluating brittleness of other rock materials needs further study. The brittleness index based on mineral content reflects the influence of the rock composition on its brittleness, while the brittleness index based on logging curves has the advantages of convenient data acquisition and fast calculation of the results, and is more suitable for field brittleness evaluation. In future research we plan to combine our index with CBM reservoir logging data and the mineral content of the coal and establish a more applicable brittleness evaluation standard.

## 6 Conclusions

1. The elastic energy accumulated in rock is the main source for its rupture and failure. The failure of absolute brittle rock is spontaneous and the accumulated elastic energy is sufficient to drive the whole failure process. In coal, however, the accumulated elastic energy is weakened by the dissipated energy before the peak and strengthened by the dissipated energy after the peak; therefore, these two energies are directly connected to the coal brittleness.
2. A new index for evaluating the coal brittleness was established in this paper from the perspective of energy evolution. The new index considers the comprehensive effect of the external loading conditions and the internal cleat system on the coal brittleness, and describes the brittleness characteristics before and after the peak. It has a solid physical basis and a straightforward calculation process.
3. The brittleness reflected by the pre-peak and post-peak strain characteristics is different in some cases, which indicates that the existing brittleness indices ( $b_4$ – $b_8$ ) established by individually considering the brittleness before or after the peak may lead to contradictory evaluation results.
4. The coal brittleness decreases with increasing confining pressure, and is significantly affected by the orientation of the cleats. When the inclination angle of the face cleats increases, the coal brittleness first increases and then decreases. The specimens with face cleat angles of  $45^\circ$  and  $90^\circ$  have the highest and lowest brittleness, respectively.
5. The AE energy curves can be divided into three types. The curve of *Rapid Fracture Type* has approximately linear lower and upper sections, with a very rapid rise between them and represent high brittleness, and the curve of the accumulation rate of AE energy has sudden changes at  $\sigma_A$  and  $\sigma_B$ . The *Plastic Fracture Type* represents low brittleness, and the curves are smooth, first concave and then convex. The *Stable Fracture Type* is the transition between *Rapid Fracture Type* and *Plastic Fracture Type*.
6. The single shear failure pattern represents low brittleness characteristics. The multi-longitudinal splitting cracks are instantaneous tensile cracks, which require low dissipation energy and can provide more paths for energy release; these cracks represent high brittleness characteristics.

**Acknowledgements** The research was supported by the Major National Science and Technology Projects (No. 2016ZX05046004-03) and the Northeast Petroleum University Innovation Foundation



for Postgraduate (No. YJSCX2017-009NEPU). We also thank Dalia Lahav-Jones, from Liwen Bianji, Edanz Group China (<http://www.liwenbianji.cn/ac>), for editing the English text of a draft of this manuscript.

## References

- Ai C, Zhang J, Li YW, Zeng J, Yang XL, Wang JG (2016) Estimation criteria for rock brittleness based on energy analysis during the rupturing process. *Rock Mech Rock Eng* 49(12):4681–4698
- Altindag R (2003) The correlation of specific energy with rock brittleness concept on rock cutting. *J S Afr I Min Metall* 103(3):163–171
- Bishop AW (1967) Progressive failure with special reference to the mechanism causing it. In: *Proceedings of the geotechnical conference, Oslo*, pp 142–150
- Blindheim OT, Bruiland A (1998) Boreability testing. Norwegian TBM tunneling 30 years of experience with TBMs in Norwegian Tunneling. Norwegian Soil and Rock Engineering Association, Trondheim, pp 29–34
- Busse J, Dreuzy JRD, Torres SG, Bringemeier D, Scheuermann A (2017) Image processing based characterisation of coal cleat networks. *Int J Coal Geol* 169:1–21
- Chen Y, Jin Y, Chen M, Yi ZC, Zheng XJ (2017) Quantitative evaluation of rock brittleness based on the energy dissipation principle, an application to type II mode crack. *J Nat Gas Sci Eng* 45:527–536
- Cheng H, Zhou XP, Zhu J, Qian Q (2016) The effects of crack openings on crack initiation, propagation and coalescence behavior in rock-like materials under uniaxial compression. *Rock Mech Rock Eng* 49:3481–3494
- Cipolla C, Warpinski NR, Mayerhofer MJ, Lolon EP, Vincent MC (2010) The relationship between fracture complexity, reservoir properties, and fracture treatment design. *SPE* 115769
- Copur H, Bilgin N, Tuncdemir H, Balci C (2003) A set of indices based on indentation test for assessment of rock cutting performance and rock properties. *J S Afr I Min Metall* 103(9):589–600
- Feng JJ, Wang EY, Chen X, Ding HC (2017) Energy dissipation rate: An indicator of coal deformation and failure under static and dynamic compressive loads. *Int J Min Sci Tech*. <https://doi.org/10.1016/j.ijmst.2017.11.006>
- Geng Z, Chen M, Jin Y, Yang S, Yi ZC, Fang X, Du XY (2016) Experimental study of brittleness anisotropy of shale in triaxial compression. *J Nat Gas Sci Eng* 36:510–518
- Guo JC, Zhao ZH, He SG, Liang H, Liu YX (2015) A new method for shale brittleness evaluation. *Environ Earth Sci* 73(10):5855–5865
- Hajiabdolmajid V, Kaiser P (2003) Brittleness of rock and stability assessment in hard rock tunneling. *Tunn Undergr Sp Tech* 18(1):35–48
- Hetényi M (1950) *Handbook of experimental stress analysis*. John Wiley, New York, pp 23–25
- Heng S, Guo YT, Yang CH, Daemen JJK, Li Z (2015) Experimental and theoretical study of the anisotropic properties of shale. *Int J Rock Mech Min* 74:58–68
- Holt RM, Fjær E, Stenebråten JF, Nes OM (2015) Brittleness of shales: relevance to borehole collapse and hydraulic fracturing. *J Petrol Sci Eng* 131:200–209
- Honda H, Sanada Y (1956) Hardness of coal. *Fuel* 35:451–455
- Hou P, Gao F, Ju Y, Liang X, Zhang ZZ, Cheng HM, Gao YN (2016a) Experimental investigation on the failure and acoustic emission characteristics of shale, sandstone and coal under gas fracturing. *J Nat Gas Sci Eng* 35:211–223
- Hou P, Gao F, Yang YG, Zhang XX, Zhang ZZ (2016b) Effect of the layer orientation on mechanics and energy evolution characteristics of shales under uniaxial loading. *Int J Min Sci Tech* 26(5):857–862
- Howell J V (1960) *Glossary of geology and related sciences*. American Geological Institute, Washington DC, pp 99–102
- Huang D, Li Y (2014) Conversion of strain energy in triaxial unloading tests on marble. *Int J Rock Mech Min Sci* 66:160–168
- Hucka V, Das B (1974) Brittleness determination of rocks by different methods. *Int J Rock Mech Min Sci Geo abstr* 11(10):389–392
- Jarvie DM, Hill RJ, Ruble TE, Pollastro RM (2007) Unconventional shale-gas systems: the mississippian barnett shale of north-central texas as one model for thermogenic shale-gas assessment. *AAPG Bull* 9(4):475–499
- Jing Y, Armstrong RT, Ramandi HL, Mostaghimi P (2016) Coal cleat reconstruction using micro-computed tomography imaging. *Fuel* 181:286–299
- Kaunda RB, Asbury B (2016) Prediction of rock brittleness using non-destructive methods for hard rock tunneling. *J Rock Mech Geo Eng* 8:533–540
- Kidybinski A (1981) Bursting liability indices of coal. *Int J Rock Mech Min Sci Geomech Abstr* 18(4):295–304
- Kong XG, Wang EY, Hu SB, Shen RX, Li XL, Zhan TQ (2015) Fractal characteristics and acoustic emission of coal containing methane in triaxial compression failure. *J Appl Geophys* 124:139–147
- Kulander BR, Dean SL (1993) Coal cleat domains and domain boundaries in the Allegheny Plateau of west Virginia. *AAPU Bull* 77(3):1374–1388
- Labuz JF, Biolzi L (1991) Class I vs Class II stability: a demonstration of size effect. *Int J Rock Mech Min* 28(2–3):199–205
- Lawn BR, Marshall DB (1979) Hardness, toughness and brittleness: an indentation analysis. *J Am Ceram Soc* 62(7/8):347–350
- Li DY, Sun Z, Xie T, Li XB, Ranjith PG (2017a) Energy evolution characteristics of hard rock during triaxial failure with different loading and unloading paths. *Eng Geol* 228:270–281
- Li XY, Lei XL, Li Q, Li XC (2017b) Experimental investigation of Sianian shale rock under triaxial stress monitored by ultrasonic transmission and acoustic emission. *J Nat Gas Sci Eng* 43:110–123
- Li YW, Jia D, Rui ZH, Peng JY, Fu CK, Zhang J (2017c) Evaluation method of rock brittleness based on statistical constitutive relations for rock damage. *J Petrol Sci Eng* 153:123–132
- Liang YP, Li QM, Gu YL, Zou QL (2017) Mechanical and acoustic emission characteristics of rock: effect of loading and unloading confining pressure at the postpeak stage. *J Nat Gas Sci Eng* 44:54–64
- Liu ZB, Sun ZD (2015) New brittleness indexes and their application in shale/clay gas reservoir prediction. *Petrol Explor Dev* 42(1):117–124
- Liu XH, Chang YR, Lu HJ, Chen BC, Li JS, Qi Y, Wang CW (2012) Optimizing fracture stimulation in low-permeability oil reservoirs in the ordos basin. *SPE* 158562
- Meng FZ, Zhou H, Zhang CQ, Xu RC, Lu JJ (2015) Evaluation methodology of brittleness of rock based on post-peak stress–strain curves. *Rock Mech Rock Eng* 48(5):1787–1805
- Meng Q, Zhang M, Han L, Pu H, Nie T (2016) Effects of acoustic emission and energy evolution of rock specimens under the uniaxial cyclic loading and unloading compression. *Rock Mech Rock Eng* 49:3873–3886
- Mishra B, Nie DC (2013) Experimental investigation of the effect of change in control modes on the post-failure behavior of coal and coal measures rock. *Int J Rock Mech Min* 60:363–369
- Mitri HS, Tang B, Simon R (1999) FE modelling of mining-induced energy release and storage rates. *J South Afr Inst Min Metall* 99(2):103–110
- Morley A (1944) *Strength of materials*. Longman Green, London, pp 71–72

- Mostaghim P, Armstrong RT, Gerami A, Hu YB, Jing Y, Kamali F, Liu M, Liu ZS, Lu X, Ramandi HL, Zamani A, Zhang YL (2017) Cleat-scale characterisation of coal: an overview. *J Nat Gas Sci Eng* 39:143–160
- Nicksiar M, Martin CD (2013) Crack initiation stress in low porosity crystalline and sedimentary rocks. *Eng Geol* 154:64–76
- Obert L, Duval WI (1967) *Rock mechanics and the design of structures in rock*. John Wiley, New York, pp 78–82
- Peng RD, Ju Y, Wang JG, Xie HP, Gao F, Mao LT (2015) Energy dissipation and release during coal failure under conventional triaxial compression. *Rock Mech Rock Eng* 48:509–526
- Protodyakonov MM (1963) Mechanical properties and drillability of rocks. In: *Proceeding of the 5th Symposium on Rock Mechanics*. Twin Cities: University of Minnesota Press, pp 103–118
- Qiao L, Ranjith PG, Long XP, Kang Y, Huang M (2015) Effects of coring directions on the mechanical properties of Chinese shale. *Arab J Geosci* 8(12):10289–10299
- Quinn JB, Quinn GD (1997) Indentation brittleness of ceramics: a fresh approach. *J Mater Sci* 32(16):4331–4346
- Rickman R, Mullen MJ, Petre JE, Grieser WV, Kundert D (2008) A practical use of shale petrophysics for stimulation design optimization: all shale plays are not clones of the Barnett Shale. In: *Proceedings of the annual technical conference (SPE 115258)*, Society of Petroleum Engineers, Denver, CO, USA, 21–24 September
- Rummel F, Fairhurst (1970) Determination of the post-failure behavior of brittle rock using a servo-controlled testing machine. *Rock Mech* 2(4):189–204
- Soliman MY, Daal J, East L (2012) Fracturing unconventional formations to enhance productivity. *J Nat Gas Sci Eng* 8:52–67
- Stavrogin AN, Tarasov BG (2001) *Experimental physics and rock mechanics*. Taylor and Francis Group, New York, pp 1342–1357
- Tarasov BG, Potvin Y (2013) Universal criteria for rock brittleness estimation under triaxial compression. *Int J Rock Mech Min* 59:57–69
- Tarasov BG, Randolph MF (2016) Improved concept of lithospheric strength and earthquake activity at shallow depths based upon the fan-head dynamic shear rupture mechanism. *Tectonophysics* 667:124–143
- Wang M, Tan C, Meng J, Yang B, Li Y (2017) Crack classification and evolution in anisotropic shale during cyclic loading tests by acoustic emission. *J Geophys Eng* 14:930–938
- Wasantha PLP, Ranjith PG, Shao SS (2014) Energy monitoring and analysis during deformation of bedded-sandstone: Use of acoustic emission. *Ultrasonics* 54(1):217–226
- Wasantha PLP, Ranjith PG, Zhang QB, Xu T (2015) Do joint geometrical properties influence the fracturing behaviour of jointed rock? An investigation through joint orientation. *Geomech Geophys Geo-energ Geo-resour* 1(1–2):3–14
- Wei HC, Li LG, Wu XM, Hu YL (2011) The analysis and theory research on the factor of multiple fractures during hydraulic fracturing of cbm wells. *Procedia Earth Plane Sci* 3:231–237
- Wu JG, Sun HS, Liu XH, Mayerhofer M, Zhang P, Wu Xiang, Zuo JL (2013) CBM development in the qinshui basin: hydraulic fracture complexities revealed by modeling analysis and microseismic monitoring. *SPE* 167045
- Wu HB, Dong SH, Huang YP, Wang HL, Chen GW (2016) Brittleness index calculation and evaluation for CBM reservoirs based on AVO simultaneous inversion. *J Appl Geophys* 134:191–198
- Xia YJ, Li LC, Tang CA, Li XY, Ma S, Li M (2017) A new method to evaluate rock mass brittleness based on stress–strain curves of class I. *Rock Mech Rock Eng* 50(5):1123–1139
- Xie HP, Li LY, Peng RD, Ju Y (2009) Energy analysis and criteria for structural failure of rocks. *J Rock Mech Geo Eng* 1(1):11–20
- Xu F, Yang CH, Guo YT, Wang L, Hou ZK, Li HR, Hu XM, Wang TT (2017) Effect of bedding planes on wave velocity and AE characteristics of the Longmaxi shale in China. *Arab J Geosci* 10(6):141
- Xue Y, Gao F, Teng T, Xing Y (2016) Effect of Gas Pressure on Rock Burst Proneness Indexes and Energy Dissipation of Coal Samples. *Geotech Geol Eng* 34(6):1737–1748
- Yagiz S (2009) Assessment of brittleness using rock strength and density with punch penetration test. *Tunn Undergr Space Technol* 24:66–74
- Yang YM, Ju Y, Li FX, Gao F, Sun HF (2016) The fractal characteristics and energy mechanism of crack propagation in tight reservoir sandstone subjected to triaxial stresses. *J Nat Gas Sci Eng* 32:415–422
- Zhang ZZ, Gao F (2015) Experimental investigation on the energy evolution of dry and water-saturated red sandstones. *Int J Min Sci Tech* 25(3):383–388
- Zhang LH, Shan BC, Zhao YL (2017) Production performance laws of vertical wells by volume fracturing in CBM reservoirs. *Nat Gas Ind B* 4(3):189–196
- Zhao XG, Cai M, Wang J, Li PF, Ma LK (2015) Objective determination of crack initiation stress of brittle rocks under compression using. *Rock Mech Rock Eng* 48:2473–2484
- Zuo JP, Liu HH, Li HT (2015) A theoretical derivation of the Hoek–Brown failure criterion for rock materials. *J Rock Mech Geo Eng* 7(4):361–366

**Publisher's Note** Springer Nature remains neutral with regard to jurisdictional claims in published maps and institutional affiliations.